MI Preprint Series
Kyushu University
The Global COE Program
Math-for-Industry Education & Research Hub

Numerical simulation of fluid movement in an hourglass by an energy-stable finite element scheme

M. Tabata

MI 2009-28

(Received August 13, 2009)

Faculty of Mathematics
Kyushu University
Fukuoka, JAPAN

Numerical simulation of fluid movement in an hourglass by an energy-stable finite element scheme

Masahisa Tabata

Department of Mathematical Sciences, Kyushu University, 6-10-1, Higashi-ku, Hakozaki, Fukuoka, 812-8581, Japan, tabata@math.kyushu-u.ac.jp

Abstract

We simulate flow movement in an hourglass occupied by two fluids with surface tension on the interface and compare the difference of movements of fluids between the non-slip and slip boundary conditions and small and large coefficients of surface tension. The simulation is carried out by an energy-stable finite element scheme developed recently by ourself.

1 Introduction

Multifluid and multiphase flows with surface tension are encountered frequently in scientific and engineering problems. Many numerical schemes have been developed and applied to those flow problems, see e.g.,[4, 10, 11, 12] and references therein. It is, however, not an easy task to construct numerical schemes, stable and convergent. To the best of our knowledge, there are no numerical schemes whose solutions are proved to converge to the exact one. There are very little discussion even for the stability of schemes [1].

Recently we have developed a class of finite element schemes based on energy-stable approximation [5, 6, 7]. In the case of no surface tension, the schemes are unconditionally stable in the energy norm. When there exists surface tension, they are proved to be stable if a quantity corresponding to L^2-norm of the curvature remains bounded in the computation. Since we do not use the maximum norm, the computation proceeds stably while the integral value is bounded even if the interface becomes singular and if the curvature becomes infinite at a point.

In this paper we apply an energy-stable finite element scheme to simulate and analyze flow movement in an hourglass. Two immiscible incompressible

viscous fluids occupy the hourglass. Surface tension is exerted on the interface of the two fluids. We consider two boundary conditions, non-slip and slip conditions, on the whole boundary of the hourglass, and also change the surface tension coefficients. We compare the difference of movements of fluids and reveal the effects of the non-slip and slip boundary conditions, and small and large coefficients of surface tension.

The contents of this paper are as follows. In Section 2 we formulate two-fluid flow problems with surface tension. In Section 3 an energy-stable finite element scheme is described. We discuss the stability in the energy norm in Section 4. In Section 5 we show numerical simulation results for the movement of fluids in an hourglass.

2 Two-fluid flows in an hourglass

Suppose that two fluids, fluid 1 and fluid 2, occupy an hourglass, see Fig. 1. They are immiscible incompressible viscous fluids. Fluid 2 (black part) is heavier than fluid 1 (white part), and it falls to the bottom. Surface tension is exerted on the interface of the two fluids. On the boundary of the hourglass the fluid is of non-slip or of slip. Both fluids are governed by the Navier-Stokes equations. We simulate numerically the movement of the fluids.

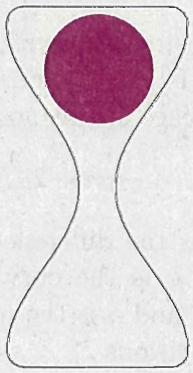

Figure 1: Two fluids in an hourglass.

We consider a two-dimensional model, whose mathematical formulation

can be written as follows. The interior of the hourglass is denoted by Ω, whose boundary Γ is smooth. Let T be a positive number. The problem is solved from time $t = 0$ until T. At the initial time $t = 0$ the domain Ω is occupied by two immiscible incompressible viscous fluids; each domain is denoted by Ω_k^0, $k = 1, 2$, whose interface $\partial\Omega_1^0 \cap \partial\Omega_2^0$ is denoted by Γ_{12}^0. Γ_{12}^0 is expressed by a closed curve. We suppose that fluid 2 is surrounded by fluid 1. At $t \in (0, T)$ the two fluids occupy unknown domains $\Omega_k(t)$, $k = 1, 2$, and the interface curve is denoted by $\Gamma_{12}(t)$. Let ρ_k and μ_k, $k = 1, 2$, be the densities and the viscosities of the two fluids. Let

$$u : \Omega \times (0, T) \to \mathbf{R}^2, \quad p : \Omega \times (0, T) \to \mathbf{R}$$

be the velocity and the pressure to be found. The Navier-Stokes equations are satisfied in each domain $\Omega_k(t)$, $k = 1, 2$, $t \in (0, T)$,

$$\rho_k \left\{ \frac{\partial u}{\partial t} + (u \cdot \nabla)u \right\} - \nabla \Big[2\mu_k D(u) \Big] + \nabla p = \rho_k f, \tag{1}$$

$$\nabla \cdot u = 0, \tag{2}$$

where $f : \Omega \times (0, T) \to \mathbf{R}^2$ is a given function, usually, the acceleration of gravity, and $D(u)$ is the strain-rate tensor defined by

$$D_{ij}(u) = \frac{1}{2} \left(\frac{\partial u_i}{\partial x_j} + \frac{\partial u_j}{\partial x_i} \right).$$

The interface Γ_{12} is assumed to move with the velocity u at that position, that is, any fluid particle on Γ_{12}^0 remains on the interface $\Gamma_{12}(t)$ at any time t. On $\Gamma_{12}(t)$, $t \in (0, T)$, interface conditions

$$[u] = 0, \qquad [-pn + 2\mu D(u)n] = \sigma_0 \kappa n \tag{3}$$

are imposed, where $[\cdot]$ means the difference of the values approached from both sides to the interface, κ is the curvature of the interface, σ_0 is the coefficient of surface tension, and n is the unit normal vector. On the whole boundary Γ the non-slip conditions

$$u = 0 \tag{4}$$

or the slip conditions

$$u \cdot n = 0, \qquad D(u)n \times n = 0 \tag{5}$$

are imposed. Initial conditions at $t = 0$ for the velocity

$$u = u^0 \tag{6}$$

are given.

The problem described above can be reformulated as follows: find functions

$$\chi : [0,1] \times (0,T) \to \mathbf{R}^2, \quad (u,p) : \Omega \times (0,T) \to \mathbf{R}^2 \times \mathbf{R}$$

satisfying for any $t \in (0,T)$,

$$\frac{\partial \chi}{\partial t} = u(\chi, t), \qquad (s \in [0,1]) \tag{7}$$

and (1) and (2) in $\Omega_k(t)$, $k = 1, 2$, with the interface conditions (3), the boundary conditions (4) or (5), and the initial conditions (6) and

$$\chi(\cdot, 0) = \chi^0, \tag{8}$$

where $\chi^0 : [0,1] \to \mathbf{R}^2$ is an initial closed curve in Ω. For any t, $\chi(1,t) = \chi(0,t)$ and

$$\mathcal{C}(t) = \{\chi(s,t); s \in [0,1]\}$$

is a closed curve in Ω, where s is a parameter. $\mathcal{C}(t)$ is nothing but the interface curve at t, and $\Omega_k(t)$, $k = 1, 2$, are defined as the exterior and the interior of $\mathcal{C}(t)$, respectively.

3 An energy-stable finite element scheme

In the paper [6] we have presented a finite element scheme based on the energy-stable approximation [8]. We apply it to the problem described in the previous section.

Let X, V, and Q be function spaces defined by

$$X = \{\chi \in H^1(0,1)^2; \chi(1) = \chi(0)\}, \quad V = H_0^1(\Omega)^2 \text{ or } H^1(\Omega)^2, \quad Q = L_0^2(\Omega),$$

where V is set to be the former space when the non-slip boundary conditions (4) are imposed and the latter when the slip boundary conditions (5) are imposed. We introduce an auxiliary function space Φ defined by

$$\Phi = L^\infty(\Omega).$$

The solution is regarded as a set of functions

$$(\chi, \rho, u, p) : (0, T) \to X \times \Phi \times V \times Q.$$

Let X_h, Φ_h, V_h, and Q_h be finite-dimensional approximation spaces of X, Φ, V, and Q. Let Δt be a time increment and $N_T = \lfloor T/\Delta t \rfloor$. At $t = n\Delta t$ we seek an approximate solution $(\chi_h^n, \rho_h^n, u_h^n, p_h^n)$ in $X_h \times \Phi_h \times V_h \times Q_h$. More precisely, these approximate function spaces are constructed as follows. Dividing the domain Ω into a union of triangles, we use $P1$, $P2$ and $P1$ finite element spaces for Φ_h, V_h and Q_h, respectively. They are fixed for all time steps n. On the other hand, X_h is composed of functions obtained by the parameterization of polygons. We denote by $\{s_i^n \in [0,1]; i = 0, \cdots, N_x^n\}$ the set of parameter values such that $s_0^n = 0$ and $s_{N_x^n}^n = 1$ and that $\{\chi_h^n(s_i^n); i = 0, \cdots, N_x^n - 1\}$ are vertices of a polygon. We set $\chi_h^n(1) = \chi_h^n(0)$. The number N_x^n may change depending on n. The notation $X_h(N_x^n)$ is used to express X_h with N_x^n parameters. We denote by $\bar{D}_{\Delta t}$ the backward difference operator, i.e.,

$$\bar{D}_{\Delta t} u_h^n = \frac{u_h^n - u_h^{n-1}}{\Delta t}.$$

Our scheme is to find

$$\{(\chi_h^n, \rho_h^n, u_h^n, p_h^n) \in X_h \times \Phi_h \times V_h \times Q_h; n = 1, \cdots, N_T\}$$

satisfying

$$\frac{\tilde{\chi}_h^n - \chi_h^{n-1}}{\Delta t} =$$

$$\begin{cases} u_h^{n-1}(\chi_h^{n-1}), & \forall s_i^{n-1},\ n = 1 \\ \frac{3}{2} u_h^{n-1}(\chi_h^{n-1}) - \frac{1}{2} u_h^{n-2}(\chi_h^{n-1} - \Delta t u_h^{n-1}(\chi_h^{n-1})), & \forall s_i^{n-1},\ n \geq 2, \end{cases} \tag{9a}$$

$$\chi_h^n = \mathcal{X}_h(\tilde{\chi}_h^n, A_h^0), \tag{9b}$$

$$\rho_h^n = \mathcal{R}_h(\chi_h^n), \tag{9c}$$

$$\left(\rho_h^{n-1} \bar{D}_{\Delta t} u_h^n + \frac{1}{2} u_h^n \bar{D}_{\Delta t} \rho_h^n, v_h\right) + a_1(\rho_h^n, u_h^{n-1}, u_h^n, v_h) + a_0(\rho_h^n, u_h^n, v_h)$$
$$+ b(v_h, p_h^n) + \Delta t\ d_h(u_h^n, v_h; C_h^n) = (\rho_h^n \Pi_h f^n, v_h) - d_h(\chi_h^n, v_h; C_h^n),$$
$$\forall v_h \in V_h, \tag{9d}$$

$$b(u_h^n, q_h) = 0, \quad \forall q_h \in Q_h \tag{9e}$$

subject to the initial conditions

$$\chi_h^0 = \Pi_h \chi^0, \quad \rho_h^0 = \mathcal{R}_h(\chi_h^0), \quad u_h^0 = \Pi_h u^0, \tag{10}$$

where Π_h is the Lagrange interpolation operator to the corresponding finite-dimensional space and A_h^0 is the area of the domain surrounded by χ_h^0. Equations (9a)-(9e) are composed of the four stages.

Stage 1. Let $(\chi_h^{n-1}, u_h^{n-1}, u_h^{n-2}) \in X_h(N_x^{n-1}) \times V_h \times V_h$ be given for $n \geq 2$. When $n = 1$, $(\chi_h^0, u_h^0) \in X_h(N_x^0) \times V_h$ is given by (10), where the definition of $\mathcal{R}_h$ is given in Stage 3. By (9a) we get a temporary function $\tilde{\chi}_h^n$,

$$\begin{aligned} (\chi_h^{n-1}, u_h^{n-1}, u_h^{n-2}) &\to \tilde{\chi}_h^n \in X_h(N_x^{n-1}), \quad n \geq 2 \\ (\chi_h^0, u_h^0) &\to \tilde{\chi}_h^1 \in X_h(N_x^0), \qquad n = 1. \end{aligned}$$

(9a) is the Adams-Bashforth approximation of (7) for $n \geq 2$, and the forward Euler approximation for $n = 1$.

Stage 2. By (9b) we fix a function χ_h^n,

$$(\tilde{\chi}_h^n, A_h^0) \to \chi_h^n \in X_h(N_x^n).$$

Here we modify $\tilde{\chi}_h^n$ to have a quasi-uniform distribution of vertices of the polygon $\tilde{\mathcal{C}}_h^n$ associated with $\tilde{\chi}_h^n$ and to keep the area of the surrounded domain to be equal to the initial area A_h^0. In the case when the distribution of vertices of $\tilde{\mathcal{C}}_h^n$ is not good, i.e., the distance of two neighboring vertices are too small or too large, we delete or add a particle and repeat the procedure to get a modified function $\bar{\chi}_h^n \in X_h(N_h^n)$, where N_x^n is the number of vertices of the modified polygon. Since the velocity u is incompressible, the area of the domain surrounded by $\mathcal{C}$ should be constant. Let $\bar{\mathcal{C}}_h^n$ be the polygon associated with $\bar{\chi}_h^n$ and $\bar{A}_h^n$ be the area. We expand or shrink $\bar{\mathcal{C}}_h^n$ from the centroid of the domain surrounded by $\bar{\chi}_h^n$ with the ratio $A_h^0/\bar{A}_h^n$ to obtain $\chi_h^n \in X_h(N_h^n)$. Those all procedures are denoted by $\mathcal{X}_h(\tilde{\chi}_h^n, A_h^0)$ in (9b).

Stage 3. By (9c) we obtain

$$\chi_h^n \to \rho_h^n \in \Phi_h$$

as follows. Once χ_h^n is known, we can define Ω_{hk}^n, $k = 1, 2$, as the exterior and the interior of the polygon $\mathcal{C}_h^n$, respectively. If the node P_i belongs to Ω_{hk}^n, we set

$$\rho_h^n(P_i) = \rho_k.$$

This procedure is denoted by $\mathcal{R}_h(\chi_h^n)$.

Stage 4. By solving a system of linear equations, (9d) and (9e), we get u_h^n and p_h^n,

$$(\chi_h^n, \rho_h^n, \rho_h^{n-1}, u_h^{n-1}) \rightarrow (u_h^n, p_h^n) \in V_h \times Q_h.$$

In (9d) the symbol $(\cdot, \cdot)$ shows the inner product in $L^2(\Omega)^2$,

$$a_1(\rho, w, u, v) = \int_\Omega \frac{1}{2}\rho\Big\{[(w \cdot \nabla)u] \cdot v - [(w \cdot \nabla)v] \cdot u\Big\} dx, \tag{11}$$

$$a_0(\rho, u, v) = \int_\Omega 2\mu(\rho) D(u) : D(v)\ dx,$$

$$b(v, q) = -\int_\Omega (\nabla \cdot v) q\ dx,$$

$$d_h(\chi, v; \mathcal{C}_h) = \sum_{i=1}^{N_x} \sigma_0 \bar{D}_{\Delta s}\chi_i \cdot \bar{D}_{\Delta s} v_i\ \frac{(s_i - s_{i-1})^2}{|\chi_i - \chi_{i-1}|},$$

$$\mu(\rho) = \mu_1 \frac{\rho_2 - \rho}{\rho_2 - \rho_1} + \mu_2 \frac{\rho - \rho_1}{\rho_2 - \rho_1},$$

and $\mathcal{C}_h^n$ is a polygon associated with χ_h^n. d_h is an approximation to a bilinear form d on the interface $\mathcal{C}$,

$$d(\chi, v; \mathcal{C}) \equiv \int_{\mathcal{C}} \sigma_0 \frac{\partial \chi}{\partial \ell} \cdot \frac{\partial v}{\partial \ell}\ d\ell,$$

where ℓ is the arclength of the interface curve $\mathcal{C}$.

Remark 1

(i) For smooth functions ρ, w, u, and v integration by parts implies the identity,

$$a_1(\rho, w, u, v) \equiv \int_\Omega \Big\{\rho(w \cdot \nabla)u + \frac{1}{2}[(w \cdot \nabla)\rho]u + \frac{1}{2}\rho(\nabla \cdot w)u\Big\} \cdot v\ dx$$
$$- \int_{\partial\Omega} \frac{1}{2}\rho(w \cdot n)(u \cdot v) ds.$$

Substituting $w = u$, and using (2) and the boundary condition (4) or (5), we obtain

$$a_1(\rho, u, u, v) = \int_\Omega \Big\{\rho(u \cdot \nabla)u + \frac{1}{2}[(u \cdot \nabla)\rho]u\Big\} \cdot v\ dx.$$

The density ρ is governed by the convection equation,

$$\frac{\partial \rho}{\partial t} + u \cdot \nabla \rho = 0. \tag{12}$$

We observe that (9d) is an approximation to a weak formulation

$$\Big(\rho \frac{\partial u}{\partial t} + \frac{1}{2} u \frac{\partial \rho}{\partial t}, v\Big) + a_1(\rho, u, u, v) + a_0(\rho, u, v) + b(v, p) \\ = (\rho f, v) - d(\chi, v; \mathcal{C}),$$

which is obtained by multiplying (12) by $u/2$ and by adding it to (1) together with the interface condition (3).

(ii) The term $\Delta t\ d_h(u_h^n, v_h; \mathcal{C}_h^n)$ is added to improve the stability. For the details we refer to [7, 9].

(iii) (9d) and (9e) compose a non-symmetric system of linear equations in u_h^n and p_h^n. We solve it by a non-symmetric solver, e.g., GMRES.

Remark 2 In place of $P1$ element for the auxiliary space Φ_h we can also use $P0$ element. When the interface curve intersects an element, the value of the element is set to be the area average of the densities in the element. We refer [7] for the details of such a choice.

4 Stability in energy

An advantage of the scheme (9) is that we can discuss the energy stability clearly. We equip the function spaces V_h, and Q_h with the norms $H^1(\Omega)^2$ and $L^2(\Omega)$, respectively. They are denoted simply by $||\cdot||_1$ and $||\cdot||_0$. In (9d) the functions ρ_h^{n-1}, ρ_h^n, u_h^{n-1}, and χ_h^n are all known. The system of (9d) and (9e) is a generalized Stokes problem in u_h^n and p_h^n. Since the P2/P1 element satisfies the inf-sup condition [2, 3], the problem is uniquely solvable.

For a series of functions $\phi_h = \{\phi_h^n\}_{n=0}^{N_T}$ in a Banach space W we prepare norms defined by

$$||\phi_h||_{\ell^\infty(W)} \equiv \max\{||\phi_h^n||_W;\ 0 \le n \le N_T\},$$

$$||\phi_h||_{\ell^2(W)} \equiv \left\{ \Delta t \sum_{n=0}^{N_T} ||\phi_h^n||_W^2 \right\}^{1/2}.$$

For a closed curve $\mathcal{C}$ we denote the L^2-norm of a function v on the curve by

$$||v||_{0,\mathcal{C}} = \sqrt{\int_{\mathcal{C}} |v|^2 d\ell}.$$

Since $\mathcal{C}_h^n$ is a polygon, we can apply the trace theorem; there exists a positive constant c such that for any $v \in H^1(\Omega)$ it holds that

$$||v||_{0,\mathcal{C}_h^n} \leq c||v||_1.$$

In general, the constant c depends on the length and the smoothness of the curve. We assume that it does not depend on h and n and that the curve is not self-intersecting for simplicity.

Hypothesis 1

(i) $\mathcal{C}_h^n$ is not self-intersecting.

(ii) There exists a positive constant c_0 independent of h and n such that

$$||v||_{0,\mathcal{C}_h^n} \leq c_0||v||_1 \quad (\forall v \in H^1(\Omega)). \tag{13}$$

Remark 3

(i) If u is continuous and satisfies the Lipschitz condition with respect to x, the ordinary differential equation (7) has a unique solution $\chi(s)$ for each s, which implies that $\mathcal{C}(t)$ is not self-intersecting. On the other hand, the approximation $\mathcal{C}_h^n$, constructed from the solution χ_h^n of (9a), may be self-intersecting, especially when Δt is large.

(ii) If $\mathcal{C}_h^n$ is divided into a number (independent of h and n) of parts and if the gradients $\nabla\chi_h^n$ are uniformly (in h and n) bounded on each part, then assumption (13) is satisfied. Although (13) looks like a rather mild assumption, it seems not so easy to give a sufficient condition for it.

Let $\chi_h \in X_h$ and $\{s_i \in [0,1];\ i = 0, \cdots, N_x\}$ be the set of parameters, $s_0 = 0, s_{N_x} = 1, \chi_h(1) = \chi_h(0)$. We define the quantity $||\chi_h||_{H^2_{0,h}(C_h)}$ by

$$||\chi_h||_{H^2_{0,h}(C_h)} = \Big\{ \sum_{i=0}^{N_x-1} |(D^2_{\Delta\ell}\chi_h)(s_i)|^2 \ell_i \Big\}^{1/2}, \tag{14}$$

where

$$\ell_i = \frac{1}{2}(\ell_{i+1/2} + \ell_{i-1/2}), \quad \ell_{i+1/2} = |\chi_h(s_{i+1}) - \chi_h(s_i)|,$$
$$(D^2_{\Delta\ell}\chi_h)(s_i) = \Big(\frac{\chi_h(s_{i+1}) - \chi_h(s_i)}{\ell_{i+1/2}} - \frac{\chi_h(s_i) - \chi_h(s_{i-1})}{\ell_{i-1/2}}\Big)/\ell_i.$$

Proposition 1 Suppose that scheme (9) has a solution $(\chi_h^n, \rho_h^n, u_h^n, p_h^n) \in X_h \times \Phi_h \times V_h \times Q_h$, $n = 0, \cdots, N_T$, and that Hypothesis 1 is satisfied. Then there exists a positive constant c independent of h and Δt such that

$$\begin{aligned} &||\sqrt{\rho_h}u_h||_{\ell^\infty(L^2)},\ ||\sqrt{\mu_h}D(u_h)||_{\ell^2(L^2)} \\ \le& c\Big\{||\sqrt{\rho_h^0}u_h^0||_0 + ||\sqrt{\rho_h}\ \Pi_h f||_{\ell^2(L^2)} + \frac{c_0\,\sigma_0}{\sqrt{\mu_{\min}}}||\chi_h||_{\ell^2(H^2_{0,h}(\mathcal{C}_h))}\Big\}, \end{aligned} \tag{15}$$

where $\mu_{\min} = \min(\mu_1, \mu_2)$.

Proof The proof is similar to that of Propsition 4.2 of [7], where the function space Φ_h is chosen to be the $P0$ element space. The key point is to get the finite difference formula in the energy norm, the first term of the right-hand side of the following identity. Substituting $v_h = u_h^n$ in (9d), we have

$$\begin{aligned} &\Big(\rho_h^{n-1}\bar{D}_{\Delta t}u_h^n + \frac{1}{2}u_h^n\bar{D}_{\Delta t}\rho_h^n, u_h^n\Big) \\ &= \bar{D}_{\Delta t}\left(\frac{1}{2}||\sqrt{\rho_h^n}u_h^n||_0^2\right) + \frac{1}{2}||\sqrt{\Delta t}\sqrt{\rho_h^{n-1}}\,\bar{D}_{\Delta t}u_h^n||_0^2 \end{aligned}$$

by virtue of the energy stable approximation [8]. We omit the remains of the proof.

Remark 4 There are correspondences,

$$||\sqrt{\rho_h}u_h||_{\ell^\infty(L^2)} \sim \max\Big\{\ \Big\{\int_\Omega \rho(t)|u(t)|^2dx\Big\}^{1/2};\ 0 \le t \le T\ \Big\},$$
$$||\chi_h||_{\ell^2(H^2_{0,2}(\mathcal{C}_h))} \sim \Big\{\int_0^T\ dt\int_{\mathcal{C}(t)}\kappa^2\ d\ell\Big\}^{1/2}.$$

Hence, (15) is a discrete version of the fact that the total energy remains bounded if the curvature is bounded in L^2-norm.

5 Numerical results

5.1 Preparation

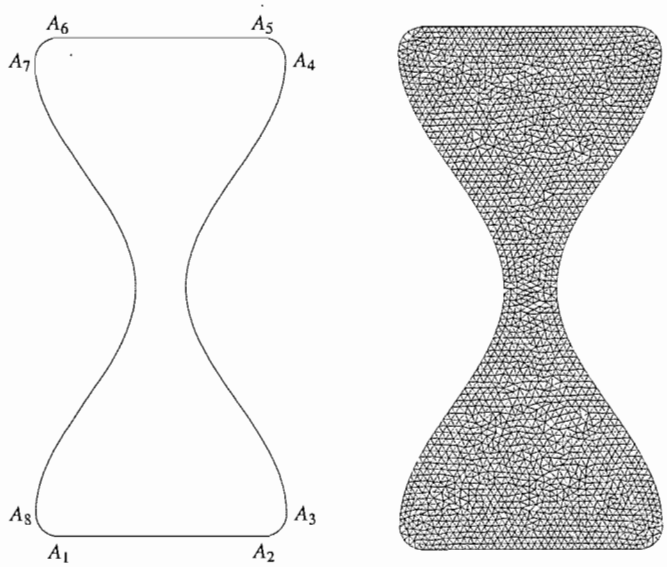

Figure 2: Domain Ω and a mesh.

The domain Ω is shown in Fig. 2, whose data are as follows. Let

$$a = 0.3, \quad b = 0.2, \quad c = 1.1, \quad r_0 = 1 - \frac{1}{c}.$$

The positions of A_i, $i = 1, \cdots, 8$, are

$$A_1(-\frac{1}{2} + r_0, 0), \ A_2(\frac{1}{2} - r_0, 0), \quad A_3(\frac{1}{2}, r_0), \qquad A_4(\frac{1}{2}, 2 - r_0),$$
$$A_5(\frac{1}{2} - r_0, 2), \quad A_6(-\frac{1}{2} + r_0, 2), \ A_7(-\frac{1}{2}, 2 - r_0), \ A_8(-\frac{1}{2}, r_0)$$

and

$$\text{curve}(A_2A_3) = \left\{ (x_1, x_2); \ x_1 = \frac{1}{2} - r_0 + r_0 \cos\theta, x_2 = r_0 + r_0 \sin\theta, \theta \in [\frac{3}{2}\pi, 2\pi] \right\}$$

$$\text{curve}(A_3A_4) = \{ (x_1, x_2); \ x_1 = a + b\cos\pi(c(x_2 - 1) + 1) \}.$$

$$\text{curve}(A_4A_5) = \left\{ (x_1, x_2); \ x_1 = \frac{1}{2} - r_0 + r_0 \cos\theta, x_2 = \frac{1}{2} - r_0 + r_0 \sin\theta, \theta \in [0, \frac{1}{2}\pi] \right\}.$$

The domain is symmetric with respect to $x_1 = 0$. We set

$$\chi^0(s) = \big(r_1 \cos 2\pi s, d + r_1 \sin 2\pi s\big), \quad r_1 = 0.3, \ d = 1.65.$$

The initial domains Ω_1^0 and Ω_2^0 are shown in Fig. 1. The initial velocity and the gravity,

$$u^0 = (0,0)^T, \quad f = (0,-1)^T$$

are given. We divide the domain Ω into the union of triangles to obtain a mesh shown in Fig. 2. The total element number N_e and the total degree of freedom N(of the velocity and the pressure) are

$$N_e = 3,974, \qquad N = 18,476.$$

In solving the problem by scheme (9), we practice the following two additional technical procedures between (9b) and (9c).

(i) We impose the condition that the interface curve should not touch the boundary Γ. When a vertex of the interface curve enters into an ϵ-neighborhood of Γ, we expel it outside the neighborhood. The distance ϵ was chosen as

$$\epsilon = 10^{-6}.$$

(ii) Subject to either non-slip or slip boundary conditions the vertical velocity component u_2 vanishes on the bottom A_1A_2 and no particles cross the boundary. In the real computation, however, some part of the interface curve may exceed the bottom A_1A_2 in (9a). When Δt is large, or even medium, it often occurs. In such a case we compute the area of the fluid part outside of Ω and expand horizontally the interior part of fluid 2 just to recover the area. This is a practical procedure not to lose the mass of fluid 2 with a resonable size of Δt.

In the following we show streamlines of velocity u, which is obtained as contours of the stream function $\psi \in H_0^1(\Omega)$ satisfying

$$-\Delta\psi = \frac{\partial u_2}{\partial x_1} - \frac{\partial u_1}{\partial x_2}. \tag{16}$$

The Poisson equation (16) is solved by the finite element method with $P1$ element on the same mesh Fig. 2. The degree of freedom N is

$$N = 2,106.$$

In all figures with streamlines the interval of contours is fixed to be 0.1. In the place where the contours are dense, the velocity is large.

The last term of the right-hand side of (15) is important for the energy stability. We use a simple notation $K(\mathcal{C}_h)$ defined by

$$K(\mathcal{C}_h) = ||\chi_h||_{\ell^2(H^2_{0,h}(\mathcal{C}_h))},$$

and the average $M(\mathcal{C}_h)$

$$M(\mathcal{C}_h) = \frac{1}{T}||\chi_h||_{\ell^1(H^2_{0,h}(\mathcal{C}_h))}$$

is also used.

5.2 The case of the non-slip boundary conditions

The non-slip boundary conditions (4) are imposed. We take the following values,

$$(\rho_1, \mu_1) = (1, 1), \quad (\rho_2, \mu_2) = (100, 2), \quad \sigma_0 = 0.1.$$

The final time T, the time increment Δt, and the total time step N_T are

$$T = 300, \quad \Delta t = \frac{1}{4}, \quad N_T = 1,200.$$

In Fig. 3 the movement of the fluids is shown from $t = 0$ until $t = 240$ at time intervals 16. In Fig. 4 the details of the movement are shown from $t = 48$ until $t = 63$ at time intervals 1. In this computation the quantities $K(\mathcal{C}_h)$ and $M(\mathcal{C}_h)$ are

$$K(\mathcal{C}_h) = 343, \quad M(\mathcal{C}_h) = 19.8.$$

Time history of energy norms $||\sqrt{\rho_h^n}u_h^n||_0$ is shown in Fig. 7 in thin line. A stable computation has been done. The minimum, maximum, and average of particle numbers N_x^n on the interfaces are

$$\min N_x = 182, \quad \max N_x = 690, \quad \text{aver} N_x = 467.$$

5.3 The case of the slip boundary conditions

The slip boundary conditions (5) are imposed. We take the following values,

$$(\rho_1, \mu_1) = (1, 1), \quad (\rho_2, \mu_2) = (100, 2), \quad \sigma_0 = 1.0.$$

The surface tension coefficient σ_0 is 10 times larger than that of the non-slip case. The final time T, the time increment Δt, and the total time step N_T are

$$T = 200, \quad \Delta t = \frac{1}{16}, \quad N_T = 3,200.$$

Since the speed of the falling fluid 2 is faster than that of the previous case, we take a smaller time increment Δt. In Fig. 5 the movement of the fluids is shown from $t = 0$ until $t = 187.5$ at time intervals 12.5. In Fig. 6 the details of the movement are shown from $t = 87.5$ until $t = 98.75$ at time intervals 0.75. In this computation the quantities $K(\mathcal{C}_h)$ and $M(\mathcal{C}_h)$ are

$$K(\mathcal{C}_h) = 240, \quad M(\mathcal{C}_h) = 16.9.$$

Time history of energy norms $||\sqrt{\rho_h^n} u_h^n||_0$ is shown in Fig. 7 in thick line. A stable computation has been done. The minimum, maximum, and average of particle numbers N_x^n on the interfaces are

$$\min N_x = 182, \quad \max N_x = 565, \quad \text{aver} N_x = 350.$$

5.4 Comparison of two cases

Fig. 7 shows the time histories of energy norms of solutions subject to the non-slip and slip boundary conditions. The speed of falling down of the latter is faster than that of the former, which is also recognized from the densities of the streamlines of Figs. 4 and 6. In both cases at the beginning fluid 2 falls rapidly to reach the narrow part of the hourglass, which produces initial large energy. In the case of non-slip boundary conditions fluid particles (of fluid 1) on the boundary do not move and stay at the same position. A neighborhood of the boundary is occupied by fluid 1, which makes the stream of fluid 2 narrow in the narrow part. Fluid 1 goes up from both sides in the narrow part, and the phenomenon is rather stable. On the other hand, in the slip case fluid 2 can approach the boundary, and it almost stops in the narrow part caused by a large surface tension. After changing the shape gradually, it passes the narrow part as a rather wide stream. In this computation fluid

1 begins to go up through the right in the narrow part aymmetrically, but the phenomenon is unstable. An oscillation of energy norm caused by this instability can be observed in Fig. 7 in thick line. In both cases there are two peaks at the time just after the falling starts from the narrow part and at the time just before the falling finishes. Those times t_1 and t_2, when the local maximums attain, were

$$t_1 = 56.75, \quad t_2 = 229.75$$

in the non-slip case, and

$$t_1 = 93.5625, \quad t_2 = 158.5625$$

in the slip case. Figs. 8 and 9 show the time histories of x_1- and x_2-coordinate of the centroid of fluid 2. In Fig. 8 we recognize again the movement of fluids in the slip case is unstable. In Fig. 9 we can see that fluid 2 passes quickly from the narrow part to the bottom in the slip case. Fig. 10 shows the time histories of the lengths of $\mathcal{C}_h^n$. Since the surface tension coefficient is larger in the slip case, the length stays shorter. Fig. 11 shows elevations of the pressure at $t = 80$ in the non-slip case (left) and at $t = 100$ in the slip case (right). To see the elevations better the figures are rotated by 180 degrees; the coordinate of the left bottom corner is $(0.5, 2)$. In the latter a large surface tension coefficient causes a high pressure in fluid 2.

6 Concluding remarks

We have simulated numerically the movement of fluids in an hourglass by an energy-stable finite element scheme. Two boundary conditions, non-slip and slip conditions, are treated. The surface tension coefficients differs in both cases. We have calculated the numerical criterion for the scheme to be stable in the energy norm, and confirmed that the computations have been done stably. We have revealed the difference of movement of fluids between the non-slip and slip boundary conditions. The effect of the difference of surface tension coefficients is also discussed.

Acknowledgements

This work was supported by the Japan Society for the Promotion of Science under Grant-in-Aid for Scientific Research (S), No.20224001 and by the Min-

istry of Education, Culture, Sports, Science and Technology of Japan under Global COE Program, Mathematics for Industry.

References

[1] E. Bänsch. Finite element discretization of the Navier-Stokes equations with a free capillary surface. *Numeische Mathematik*, Vol. 88, pp. 203–235, 2001.

[2] F. Brezzi and M. Fortin. *Mixed and Hybrid Finite Element Methods.* Springer, New York, 1991.

[3] V. Girault and P. A. Raviart. *Finite Element Methods for Navier-Stokes Equations, Theory and Algorithms*, Springer, New York, 1986.

[4] S. Osher and R. P. Fedkiw. Level set methods: an overview and some recent results. *Journal of Computational Physics*, Vol. 169, pp. 463–502, 2001.

[5] M. Tabata. Numerical simulation of Rayleigh-Taylor problems by an energy-stable finite element scheme. In B.-Y. Guo and Z.-C. Shi, editors, *Proceedings of The Fourth International Workshop on Scientific Computing and Applications*, pp. 63–73. Science Press, Beijing, 2007.

[6] M. Tabata. Energy stable finite element schemes and their applications to two-fluid flow problems. In P. Wesseling, E. Oñate, and J. Périaux, editors, *Proceedings of European Conference on Computational Fluid Dynamics*, pp. 379/1–10. TU Delft, The Netherlands, 2006.

[7] M. Tabata. Finite element schemes based on energy-stable approximation for two-fluid flow problems with surface tension. *Hokkaido Mathematical Journal*, Vol. 36, No. 4, pp. 875–890, 2007.

[8] M. Tabata and S. Kaizu. Finite element schemes for two-fluids flow problems. In Z.-C. Shi and H. Okamoto, editors, *Proceedings of The Seventh China-Japan Seminar on Numerical Mathematics*, pp. 139–148. Science Press, Beijing, 2006.

[9] M. Tabata and D. Tagami. A finite element analysis of a linearized problem of the Navier-Stokes equations with surface tension. *SIAM Journal on Numerical Analysis*, Vol. 38, pp. 40–57, 2000.

[10] T. E. Tezduyar, M. Behr, and J. Liou. A new strategy for finite element computations involving boundaries and interfaces - the deforming-spatial-domain /space-time procedure: I. *Computer Methods in Applied Mechanics and Engineering*, Vol. 94, pp. 339-351, 1992.

[11] G. Tryggvason, B. Bunner, A. Esmaeeli, D. Juric, N. Al-Rawahi, W. Tauber, J. Han, S. Nas, and Y.-J. Jan. A front-tracking method for the computations of multiphase flow. *Journal of Computational Physics*, Vol. 169, pp. 708–759, 2001.

[12] T. Yabe, F. Xiao, and T. Utsumi. The contrained interpolation profile method for multiphase analysis. *Journal of Computational Physics*, Vol. 169, pp. 556–593, 2001.

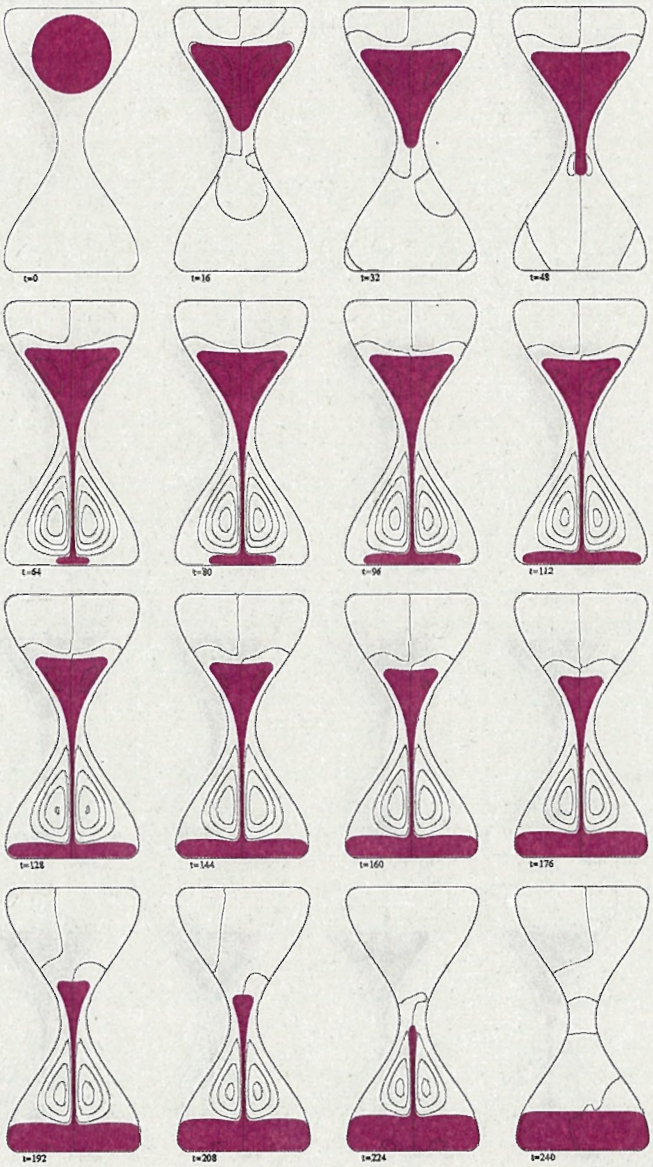

Figure 3: Interfaces and streamlines at $t = 0, 16, \cdots, 240$ subject to the non-slip boundary conditions.

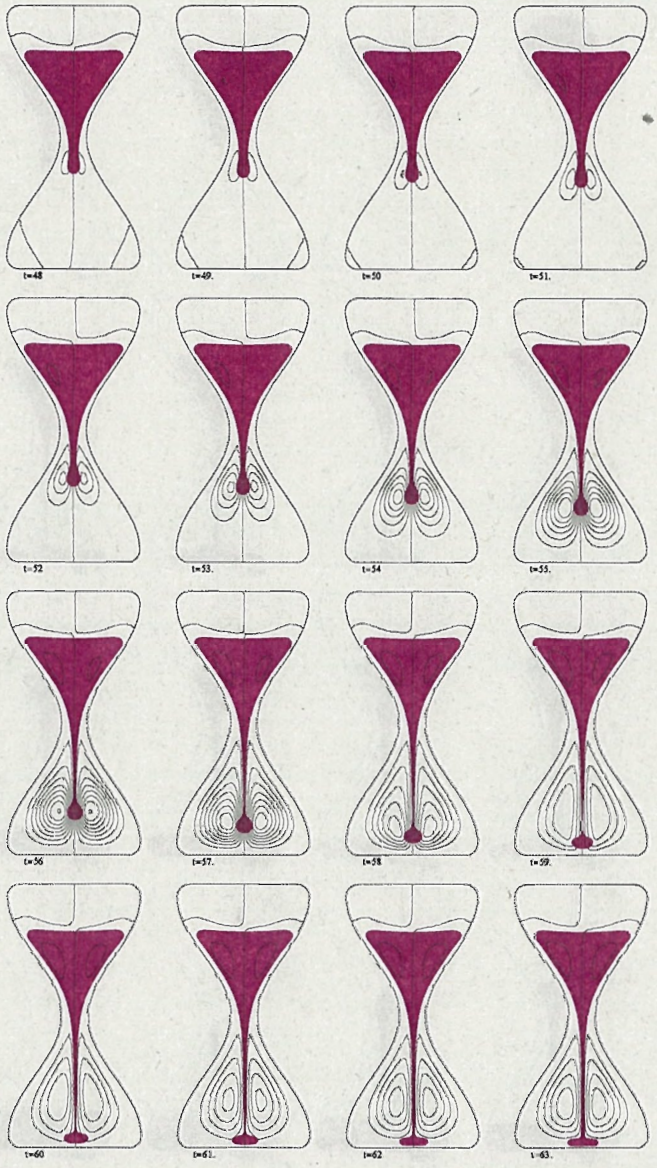

Figure 4: Interfaces and streamlines at $t = 48, 49, \cdots, 63$ subject to the non-slip boundary conditions.

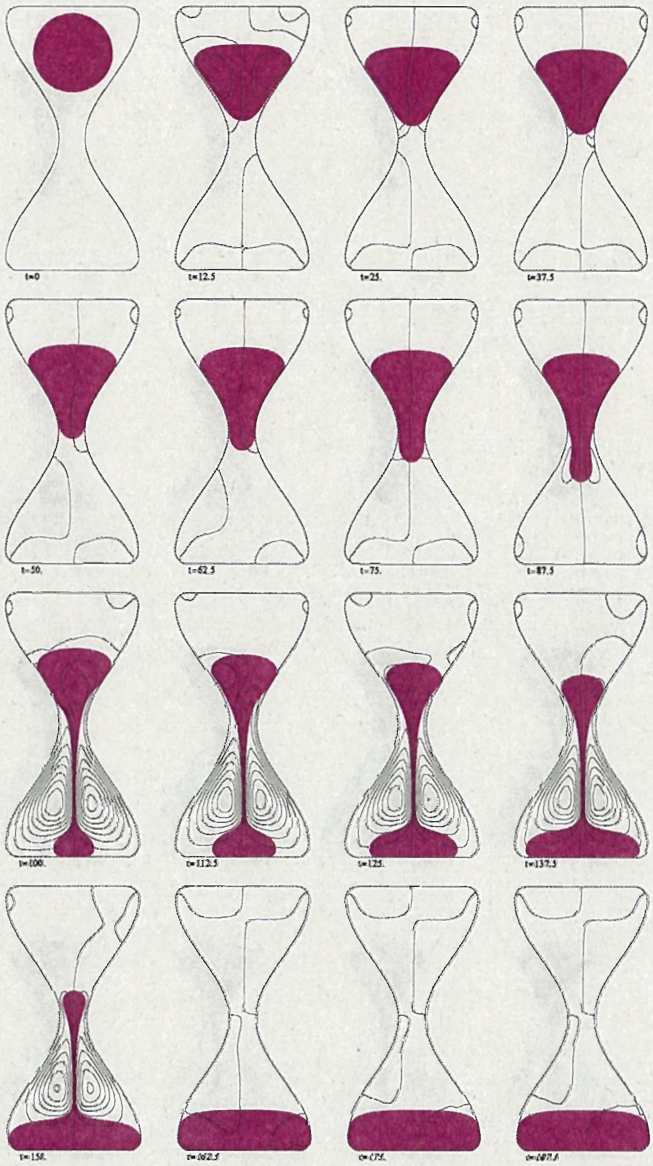

Figure 5: Interfaces and streamlines at $t = 0, 12.5, \cdots, 187.5$ subject to the slip boundary conditions.

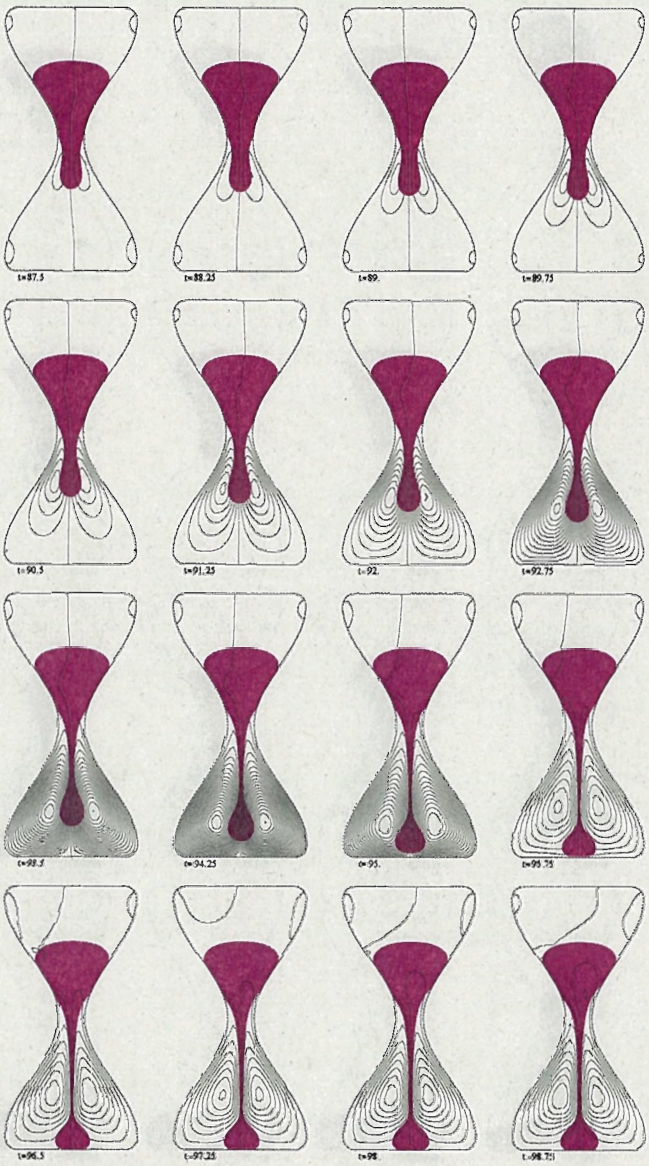

Figure 6: Interfaces and streamlines at $t = 87.5, 88.25, \cdots, 98.75$ subject to the slip boundary conditions.

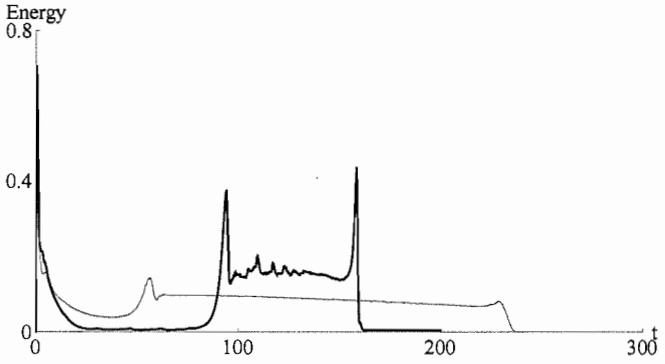

Figure 7: Time histories of energy norms in non-slip (thin) and slip (thick) boundary conditions.

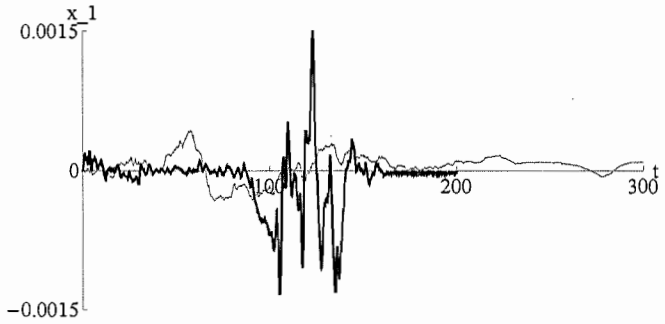

Figure 8: Time histories of x_1-coordinate of the centroid of fluide 2 in non-slip (thin) and slip (thick) cases.

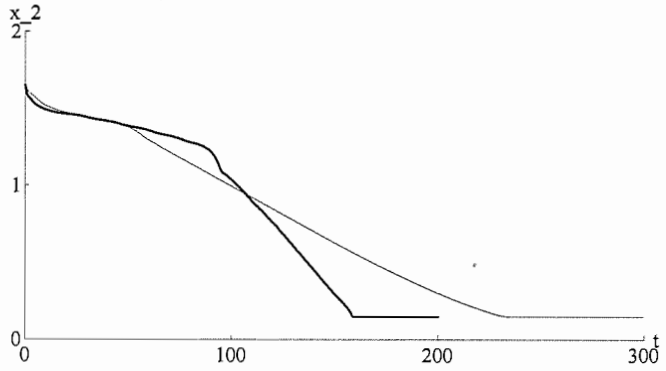

Figure 9: Time histories of x_2-coordinate of the centroid of fluide 2 in non-slip (thin) and slip (thick) cases.

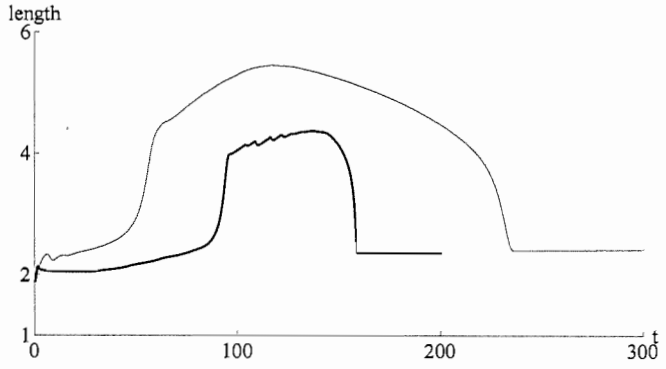

Figure 10: Time histories of the length of the interface curve in non-slip (thin) and slip (thick) cases.

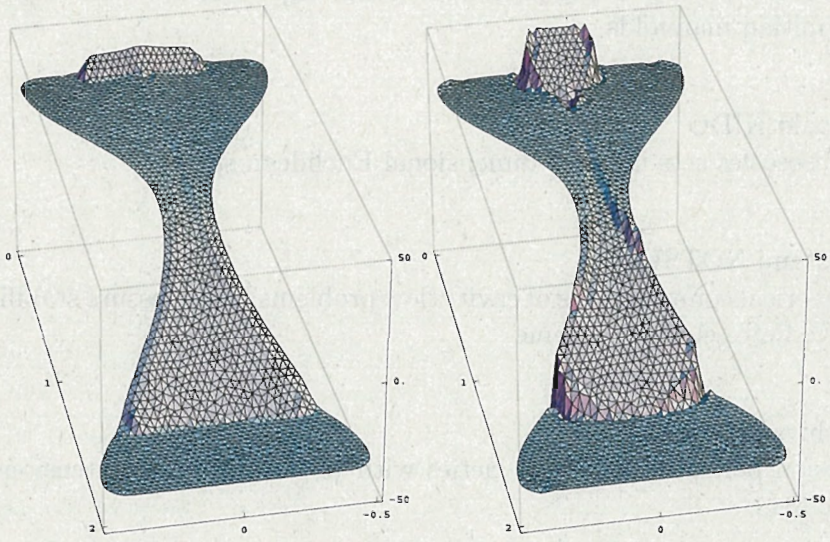

Figure 11: Elevations of the pressure at $t = 80$ in non-slip (left) and at $t = 100$ slip (right) cases .

List of MI Preprint Series, Kyushu University

The Global COE Program
Math-for-Industry Education & Research Hub

MI

MI2008-1 Takahiro ITO, Shuichi INOKUCHI & Yoshihiro MIZOGUCHI
Abstract collision systems simulated by cellular automata

MI2008-2 Eiji ONODERA
The intial value problem for a third-order dispersive flow into compact almost Hermitian manifolds

MI2008-3 Hiroaki KIDO
On isosceles sets in the 4-dimensional Euclidean space

MI2008-4 Hirofumi NOTSU
Numerical computations of cavity flow problems by a pressure stabilized characteristic-curve finite element scheme

MI2008-5 Yoshiyasu OZEKI
Torsion points of abelian varieties with values in nfinite extensions over a p-adic field

MI2008-6 Yoshiyuki TOMIYAMA
Lifting Galois representations over arbitrary number fields

MI2008-7 Takehiro HIROTSU & Setsuo TANIGUCHI
The random walk model revisited

MI2008-8 Silvia GANDY, Masaaki KANNO, Hirokazu ANAI & Kazuhiro YOKOYAMA
Optimizing a particular real root of a polynomial by a special cylindrical algebraic decomposition

MI2008-9 Kazufumi KIMOTO, Sho MATSUMOTO & Masato WAKAYAMA
Alpha-determinant cyclic modules and Jacobi polynomials

MI2008-10 Sangyeol LEE & Hiroki MASUDA
Jarque-Bera Normality Test for the Driving Lévy Process of a Discretely Observed Univariate SDE

MI2008-11 Hiroyuki CHIHARA & Eiji ONODERA
A third order dispersive flow for closed curves into almost Hermitian manifolds

MI2008-12 Takehiko KINOSHITA, Kouji HASHIMOTO and Mitsuhiro T. NAKAO
On the L^2 a priori error estimates to the finite element solution of elliptic problems with singular adjoint operator

MI2008-13 Jacques FARAUT and Masato WAKAYAMA
Hermitian symmetric spaces of tube type and multivariate Meixner-Pollaczek polynomials

MI2008-14 Takashi NAKAMURA
Riemann zeta-values, Euler polynomials and the best constant of Sobolev inequality

MI2008-15 Takashi NAKAMURA
Some topics related to Hurwitz-Lerch zeta functions

MI2009-1 Yasuhide FUKUMOTO
Global time evolution of viscous vortex rings

MI2009-2 Hidetoshi MATSUI & Sadanori KONISHI
Regularized functional regression modeling for functional response and predictors

MI2009-3 Hidetoshi MATSUI & Sadanori KONISHI
Variable selection for functional regression model via the L_1 regularization

MI2009-4 Shuichi KAWANO & Sadanori KONISHI
Nonlinear logistic discrimination via regularized Gaussian basis expansions

MI2009-5 Toshiro HIRANOUCHI & Yuichiro TAGUCHII
Flat modules and Groebner bases over truncated discrete valuation rings

MI2009-6 Kenji KAJIWARA & Yasuhiro OHTA
Bilinearization and Casorati determinant solutions to non-autonomous 1+1 dimensional discrete soliton equations

MI2009-7 Yoshiyuki KAGEI
Asymptotic behavior of solutions of the compressible Navier-Stokes equation around the plane Couette flow

MI2009-8 Shohei TATEISHI, Hidetoshi MATSUI & Sadanori KONISHI
Nonlinear regression modeling via the lasso-type regularization

MI2009-9 Takeshi TAKAISHI & Masato KIMURA
Phase field model for mode III crack growth in two dimensional elasticity

MI2009-10 Shingo SAITO
Generalisation of Mack's formula for claims reserving with arbitrary exponents for the variance assumption

MI2009-11 Kenji KAJIWARA, Masanobu KANEKO, Atsushi NOBE & Teruhisa TSUDA
Ultradiscretization of a solvable two-dimensional chaotic map associated with the Hesse cubic curve

MI2009-12 Tetsu MASUDA
Hypergeometric τ -functions of the q-Painlevé system of type $E_8^{(1)}$

MI2009-13 Hidenao IWANE, Hitoshi YANAMI, Hirokazu ANAI & Kazuhiro YOKOYAMA
A Practical Implementation of a Symbolic-Numeric Cylindrical Algebraic Decomposition for Quantifier Elimination

MI2009-14 Yasunori MAEKAWA
On Gaussian decay estimates of solutions to some linear elliptic equations and its applications

MI2009-15 Yuya ISHIHARA & Yoshiyuki KAGEI
Large time behavior of the semigroup on L^p spaces associated with the linearized compressible Navier-Stokes equation in a cylindrical domain

MI2009-16 Chikashi ARITA, Atsuo KUNIBA, Kazumitsu SAKAI & Tsuyoshi SAWABE
Spectrum in multi-species asymmetric simple exclusion process on a ring

MI2009-17 Masato WAKAYAMA & Keitaro YAMAMOTO
Non-linear algebraic differential equations satisfied by certain family of elliptic functions

MI2009-18 Me Me NAING & Yasuhide FUKUMOTO
Local Instability of an Elliptical Flow Subjected to a Coriolis Force

MI2009-19 Mitsunori KAYANO & Sadanori KONISHI
Sparse functional principal component analysis via regularized basis expansions and its application

MI2009-20 Shuichi KAWANO & Sadanori KONISHI
Semi-supervised logistic discrimination via regularized Gaussian basis expansions

MI2009-21 Hiroshi YOSHIDA, Yoshihiro MIWA & Masanobu KANEKO
Elliptic curves and Fibonacci numbers arising from Lindenmayer system with symbolic computations

MI2009-22 Eiji ONODERA
A remark on the global existence of a third order dispersive flow into locally Hermitian symmetric spaces

MI2009-23 Stjepan LUGOMER & Yasuhide FUKUMOTO
Generation of ribbons, helicoids and complex scherk surface in laser-matter Interactions

MI2009-24 Yu KAWAKAMI
Recent progress in value distribution of the hyperbolic Gauss map

MI2009-25 Takehiko KINOSHITA & Mitsuhiro T. NAKAO
On very accurate enclosure of the optimal constant in the a priori error estimates for H_0^2-projection

MI2009-26 Manabu YOSHIDA
Ramification of local fields and Fontaine's property (Pm)

MI2009-27 Yu KAWAKAMI
Value distribution of the hyperbolic Gauss maps for flat fronts in hyperbolic three-space

MI2009-28 Masahisa TABATA
Numerical simulation of fluid movement in an hourglass